

Minimal Kinematic Constraints and m_{T2}

Hsin-Chia Cheng and Zhenyu Han

Department of Physics, University of California, Davis, CA 95616

E-mail: cheng@physics.ucdavis.edu, zhenyuhan@physics.ucdavis.edu

ABSTRACT: We clarify the relation between the variable m_{T2} and the method of kinematic constraints, both of which can be used for mass determination in events with two missing (dark matter) particles at hadron colliders. We identify a set of minimal kinematic constraints, including the mass shell conditions for the missing particles and their mother particles, as well as the constraint from the measured missing transverse momentum. We show that m_{T2} is the boundary of the mass region consistent with the minimal constraints. From this point of view, we also obtained a more efficient algorithm for calculating m_{T2} . When more constraints are available in the events, we can develop more sophisticated mass determination methods starting from the m_{T2} constraint. In particular, we discuss cases when each decay chain contains two visible particles.

Contents

1. Introduction	1
2. m_{T2} from kinematic constraints	4
2.1 The definition of m_{T2}	4
2.2 m_{T2} from minimal kinematic constraints	6
2.3 Calculating m_{T2}	7
3. Mass determination using m_{T2}	9
4. Discussion and conclusions	14
A. The bisection method for calculating m_{T2}	19

1. Introduction

Many extensions beyond the standard model (SM) predict a dark matter candidate, that is, a massive stable particle interacting weakly with the SM particles. These include the minimal supersymmetric standard model (MSSM) with R-parity, universal extra dimension (UED) models [1] with KK-parity, little Higgs models with T-parity (LHT) [2] and so forth. A common feature of these models is that they all possess an exact parity, under which the SM particles are even and some new physical states are odd. Therefore the lightest parity-odd particle is stable and plays the role of the dark matter candidate. At a collider, the parity odd particles must be produced in pairs. Each of them will then go through cascade decays ending at the stable particle. Because it is weakly interacting, the stable particle will escape the detector without being detected, leaving missing energy signals.

The Large Hadron Collider (LHC) will start collisions and collecting data very soon. Once large missing energy signals are detected at the LHC, it is crucial to investigate the properties of the new particles involved in the events, in order to identify the underlying theory, as well as to determine if the invisible particle is a viable dark matter candidate. Of particular interest are the masses of the new particles, including the invisible one. Due to the fact that there are always two or more invisible particles in each of such

events, mass determination will be a difficult task. For a hadron collider, the total momentum in the beam direction is not measured, making it even more challenging.

Distributions of some simple kinematic variables such as \not{p}_T , E_T and M_{eff} [3] have been used to give estimates of the masses of the new particles. However, these variables are mostly sensitive to the mass differences of the new particles, instead of the absolute mass scale. On the other hand, the total production cross section and the full likelihood method require knowledge of the underlying physics such as the matrix elements, and hence are model-dependent. Measurements of the new particle properties should be the first step towards uncovering the underlying theory instead of the other way around. It is therefore desirable to be able to determine masses in a model-independent way by using only kinematics. Traditionally, this has been done by looking for the edges/endpoints of various invariant mass distributions of the visible particles [4]. The positions of these edges/endpoints are functions of the masses of the particles involved in the decay chains. If the decay chains are long enough, there may be enough independent invariant mass endpoints involving the visible SM particles, which allows one to reverse the relations to obtain the masses. Nevertheless, this method applies to individual decay chains and can only work for the long decay chains (4 or more on-shell particles in a decay chain). It does not utilize all information in the events such as the measured missing transverse momentum. Consequently, a large number of events are required to distinguish and measure all edges/endpoints in order to achieve a reasonable determination of the masses. It is therefore important to develop new mass determination techniques which are more powerful and can also be applied to shorter decay chains for events involving invisible particles.

Recently, along this direction, two kinds of mass determination techniques have been proposed. One of them utilizes the “kinematic constraints” [5, 6, 7]. Assuming that the event topology is known, one can try to reconstruct the kinematics event by event, by imposing the mass-shell constraints and the constraint from the measured missing transverse momentum, \not{p}_T . Depending on how many constraints that we can impose, the detailed methods can be different. In Ref. [6], the authors considered events with two identical decay chains, each containing two visible particles. Assuming that all intermediate particles are on-shell, the two invisible particles’ momenta can be solved for given trial masses. Requiring the solutions to be physical, one can determine the masses by examining the number of solvable events for all possible trial masses. Another method requires longer decay chains and therefore more constraints. It is then possible to combine multiple events and solve directly for the masses and the momenta, without assuming any trial masses [7]. This technique has been combined with the edge/endpoint method to achieve further improvement [8].

In a seemingly parallel approach, several authors have studied mass determination

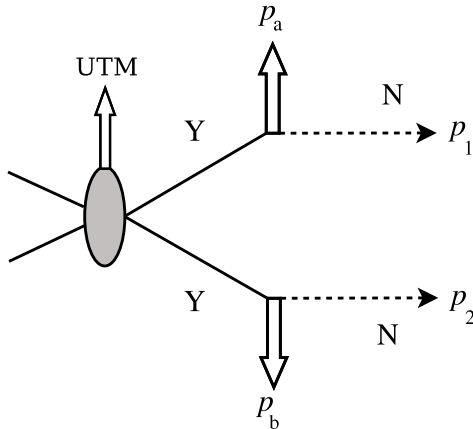


Figure 1: An event with two invisible particles N , each from a decay of a heavy particle Y .

methods using the variable m_{T2} [9], which is sometimes called the *stransverse mass*. m_{T2} is defined event by event as a function of the invisible particle mass. Its endpoint or maximal value over many events, denoted by m_{T2}^{\max} , gives an estimate of the mother particle’s mass in the beginning of the decay chain. When the invisible particle’s mass is unknown, one has to use a trial mass to calculate m_{T2} and only obtains an estimate of the mass difference. However, it has been shown in Ref. [10] that if the two mother particles decay through three-body decays to the invisible particles, a “kink” occurs on the m_{T2}^{\max} curve as a function of the trial mass. The position of the kink is actually at the true value of the invisible particle mass, which allows us to simultaneously determine the masses of both the invisible particle and its mother particle. A generalized study of the kink method is available in Ref. [11].

The purpose of this paper is to clarify the relation between the two mass determination techniques, *i.e.*, the one using kinematic constraints and the one using the variable m_{T2} . An apparent difference between the two approaches is that the former uses the 4-momenta of the visible particles, while the latter is defined solely on the plane transverse to the beam direction. Nevertheless, due to the lack of total momentum measurement in the beam direction, the longitudinal momenta of the two invisible particles can be arbitrarily chosen, offsetting some of the information obtained from the visible particles’ longitudinal momenta. As a consequence, m_{T2} is equivalent to the “minimal” kinematic constraints discussed below.

We illustrate our definition of “minimal” constraints in Fig. 1. Two mother particles of the same mass, m_Y , each decays to a dark matter particle of mass m_N , plus some visible particles, either directly or through other on-shell particles. Since the

two masses are unknown, we have to assume some trial masses, denoted by μ_Y and μ_N . Upstream transverse momentum (UTM) can be present but it must be known. The “minimal” constraints are then defined as the mass-shell conditions from μ_Y and μ_N , plus the constraint from the measured \not{p}_T . Obviously, for a given trial mass of the invisible particle μ_N , the mother particle cannot be too light otherwise we cannot obtain physical momenta for the invisible particles. As we will see, we can satisfy the minimal constraints and obtain physical momenta if and only if $\mu_Y \geq m_{T2}$. We note that this fact has been implicitly used in Ref. [12], and we give a detailed account in this article. An important by-product of our discussion is that we develop a new algorithm to calculate m_{T2} which is 5–9 times as fast as the currently available program.

Since m_{T2} corresponds to the minimal kinematic constraints, it can serve as a starting point for mass determination with more complicated topologies. The aforementioned “kink” method is an example. The m_{2C} variable defined in Ref. [12] is another example, in which the authors combine m_{T2} with the measurement of the invariant mass distribution endpoint. We will give more examples in this article.

The paper is organized as follows. In the next section, after reviewing the definition of m_{T2} , we prove that it is equivalent to the minimal kinematic constraints. Deriving m_{T2} from kinematic constraints also provides us a fast algorithm for calculating m_{T2} , which is presented in Section 2.3. In Section 3, we discuss some mass determination methods from our understanding of the relation between m_{T2} and kinematic constraints. A more general discussion of kinematic constraints and conclusions are contained in Section 4.

2. m_{T2} from kinematic constraints

2.1 The definition of m_{T2}

The definition of m_{T2} is motivated from the transverse mass m_T , which is defined for events with one invisible particle at a hadron collider. In this case, the measured missing transverse momentum is equal to the transverse momentum of the invisible particle. m_T has been used, for example, in the measurement of the W boson mass in the decay $W \rightarrow \ell\nu$. Using the notation of the W decay, m_T is defined by

$$m_T^2 = m_\ell^2 + m_\nu^2 + 2(E_T^\ell E_T^\nu - \mathbf{p}_T^\ell \cdot \mathbf{p}_T^\nu), \quad (2.1)$$

where m_ℓ and m_ν are respectively the masses of the lepton and the neutrino, and \mathbf{p}_T^ℓ and \mathbf{p}_T^ν are their transverse momenta. The beams are chosen to be along the z direction, therefore $\mathbf{p}_T = (p_x, p_y)$. E_T^ℓ , E_T^ν are transverse energies defined by

$$E_T^\ell = \sqrt{m_\ell^2 + |\mathbf{p}_T^\ell|^2}, \quad E_T^\nu = \sqrt{m_\nu^2 + |\mathbf{p}_T^\nu|^2}. \quad (2.2)$$

For convenience, we use α to denote the 2+1 dimensional momentum, $\alpha = (E_T, \mathbf{p}_T)$, while the 4-momentum is denoted by p . In the 2+1 dimensional notation, the transverse mass is given by

$$m_T^2 = (\alpha_\ell + \alpha_\nu)^2. \quad (2.3)$$

The following relation is always satisfied for the physical momenta p^ℓ , p^ν and the corresponding 2+1 dimensional momenta:

$$(p_\ell + p_\nu)^2 \geq (\alpha_\ell + \alpha_\nu)^2. \quad (2.4)$$

The equality holds if and only if ℓ and ν have the same rapidity, which is given by

$$\eta = \frac{1}{2} \ln \left(\frac{E + p_z}{E - p_z} \right). \quad (2.5)$$

When the event contains two or more missing particles, we can no longer calculate the transverse mass because the transverse momentum of the individual missing particle is unknown. As mentioned in the Introduction, a particular interesting case is that there are two decay chains in the event, each ends with an invisible particle of species N . We further assume that each decay chain also contains a particle of species Y , decaying to the particle N plus some visible particles. This is illustrated in Fig. 1, where we have labeled the invisible particles as 1 and 2, and summed the visible 4-momenta to p_a and p_b for the two decay chains respectively. We will treat a and b as two particles whose masses may vary from event to event. There can be other upstream transverse momentum (UTM) from, for example, initial state radiation or heavier particle decays. However, it is important that 1 and 2 are the only invisible particles.

Comparing with the W decay example, we see two difficulties associated with the above decay chains. First, m_N , the mass of the particle N is *a priori* unknown. Second, only the sum of the two invisible particles' transverse momenta is measured. These difficulties motivated the authors of Ref. [9] to define a quantity m_{T2} , using a trial N mass (denoted by μ_N) and minimizing over all possible partitions of the measured transverse momentum:

$$\begin{aligned} m_{T2}^2(\mu_N) &\equiv \min_{\mathbf{p}_T^1 + \mathbf{p}_T^2 = \cancel{\mathbf{p}}_T} \left[\max\{m_T^2(\mathbf{p}_T^1, \mathbf{p}_T^a; \mu_N), m_T^2(\mathbf{p}_T^2, \mathbf{p}_T^b; \mu_N)\} \right] \\ &= \min_{\mathbf{p}_T^1 + \mathbf{p}_T^2 = \cancel{\mathbf{p}}_T} \left[\max\{(\alpha_1 + \alpha_a)^2, (\alpha_2 + \alpha_b)^2\} \right], \end{aligned} \quad (2.6)$$

where in the second line we have rewritten the transverse mass using the 2+1 dimensional notation. By definition, m_{T2} is an event-by-event quantity depending on the trial mass μ_N . Therefore, strictly speaking it is not a variable, but a function of μ_N .

For a given μ_N , we can examine the m_{T2} distribution for a large number of events, which in general has an end point. As discussed in Ref. [9], the m_{T2} end point gives the correct mass of the particle Y when the trial mass is equal to the true mass of the missing particle N , $\mu_N = m_N$. We can therefore use m_{T2} to determine m_Y if m_N is known, analogous to the W mass measurement. Moreover, it has recently been shown [10] that, even if m_N is unknown, in some cases, when we plot the m_{T2} endpoint as a function of the trial mass μ_N , there is a kink at $\mu_N = m_N$. Thus both m_N and m_Y can be determined by studying the m_{T2} distribution.

We will discuss mass determination using m_{T2} in Section 3. Before that, we first give an alternative definition of m_{T2} , using the concept of kinematic constraints.

2.2 m_{T2} from minimal kinematic constraints

By kinematic constraints, we mean two kinds of constraints imposing on the 4-momenta of the invisible particles: the mass shell constraints and the measured missing transverse momentum constraints. Specifically, for the event in Fig. 1, we can write down the following equations:

$$\begin{aligned} p_1^2 &= p_2^2 = \mu_N^2, \\ (p_1 + p_a)^2 &= (p_2 + p_b)^2 = \mu_Y^2, \\ p_1^x + p_2^x &= \cancel{p}^x, \quad p_1^y + p_2^y = \cancel{p}^y, \end{aligned} \tag{2.7}$$

where μ_Y is a trial mass for the particle Y . We call this set of constraints “minimal” because they correspond to the shortest decay chains. Note that for a given set of (μ_N, μ_Y) , the system contains only 6 equations, which are not enough for completely determining p_1 and p_2 . Nevertheless, Eqs. (2.7) still constrain the possible (μ_N, μ_Y) . In particular, we will shortly see that for a given μ_N , Eqs. (2.7) can be satisfied for some physical momenta p_1 and p_2 if and only if $\mu_Y > m_{T2}(\mu_N)$. Here, a momentum is “physical” if all of its components are real and the energy component is positive. In other words, $m_{T2}(\mu_N)$ can be defined as the boundary of the consistent region on the (μ_N, μ_Y) plane, subject to the minimal constraints in Eqs. (2.7). This fact has been used in Ref. [12] but without a clear proof.

First, it is easy to show that μ_Y cannot go below m_{T2} for a fixed μ_N . For any (μ_N, μ_Y) in the consistent mass region, there exist physical p_1 and p_2 satisfying Eqs. (2.7). On the other hand, from Eq. (2.4), we have

$$\mu_Y^2 = (p_1 + p_a)^2 = (p_2 + p_b)^2 \geq \max\{(\alpha_1 + \alpha_a)^2, (\alpha_2 + \alpha_b)^2\}. \tag{2.8}$$

By definition, m_{T2} is the minimum of $\max\{(\alpha_1 + \alpha_a)^2, (\alpha_2 + \alpha_b)^2\}$ over all partitions of the missing transverse momentum. Therefore, we conclude that $\mu_Y \geq m_{T2}(\mu_N)$.

For the reverse direction we need to prove that for a given μ_N , the point $(\mu_N, m_{T2}(\mu_N))$ is indeed in the consistent mass region. By the definition of m_{T2} , there exist physical 2+1 dimensional momenta satisfying

$$\begin{aligned}\alpha_1^2 &= \alpha_2^2 = \mu_N^2, \\ m_{T2}^2 &= (\alpha_1 + \alpha_a)^2 \geq (\alpha_2 + \alpha_b)^2, \\ p_1^x + p_2^x &= p^x, \quad p_1^y + p_2^y = p^y.\end{aligned}\tag{2.9}$$

Note that if $(\alpha_1 + \alpha_a)^2 < (\alpha_2 + \alpha_b)^2$, we can simply exchange the labels. Given α_1 and α_2 , we can arbitrarily choose p_{1z} and p_{2z} (or equivalently, the rapidities η_1, η_2) of particles 1 and 2, and Eqs. (2.9) are still satisfied. In particular, we can choose a p_{1z} such that $\eta_1 = \eta_a$. In this case we have $(p_1 + p_a)^2 = (\alpha_1 + \alpha_a)^2 = m_{T2}^2$. As for the other decay chain, if $(\alpha_2 + \alpha_b)^2 = m_{T2}^2$, we choose $\eta_2 = \eta_b$; if $(\alpha_2 + \alpha_b)^2 < m_{T2}^2$, we have $(p_2 + p_b)^2 < m_{T2}^2$ when $\eta_2 = \eta_b$, and $(p_2 + p_b)^2 \rightarrow \infty$ when $\eta_2 \rightarrow \pm\infty$, as a result, there exists an η_2 such that $(p_2 + p_b)^2 = m_{T2}^2$. In this way we obtain physical momenta p_1 and p_2 which satisfy Eqs. (2.7) with $\mu_Y = m_{T2}(\mu_N)$. This concludes our proof.

2.3 Calculating m_{T2}

In the previous subsection, we have shown that m_{T2} is the boundary of the mass region consistent with the minimal kinematic constraints. This provides us not only a way to understand m_{T2} , but also an effective method of *calculating* it.

We start by discussing how to determine if a mass pair (μ_N, μ_Y) is consistent with the constraints in Eqs. (2.7). Note that m_{T2} is invariant under any independent longitudinal boosts for the particles a and b . This allows us to set p_a^z and p_b^z to zero for convenience. We also assume $m_a > 0$ and $m_b > 0$ for the moment.

We first consider the decay chain involving particles 1 and a . From the mass shell constraints $p_1^2 = \mu_N^2$ and $(p_1 + p_a)^2 = \mu_Y^2$, we can express E_1 in terms of p_1^x and p_1^y :

$$E_1 = \frac{p_a^x}{E_a} p_1^x + \frac{p_a^y}{E_a} p_1^y + \frac{\mu_Y^2 - \mu_N^2 - m_a^2}{2E_a}.\tag{2.10}$$

In order to have p_1 physical, we must have

$$-p_1^{z2} = -(E_1^2 - p_1^{x2} - p_1^{y2} - \mu_N^2) \leq 0.\tag{2.11}$$

Eq. (2.11) imposes a constraint on possible p_1^x and p_1^y . It is straightforward to show that the allowed (p_1^x, p_1^y) is the region enclosed by an ellipse. We will distinguish an ellipse and the region that it encloses by calling the latter an “elliptical region.” The size of the ellipse depends on μ_Y monotonically. In particular, it shrinks to zero when $\mu_Y = \mu_N + m_a$, in which case all three particles have the same velocity.

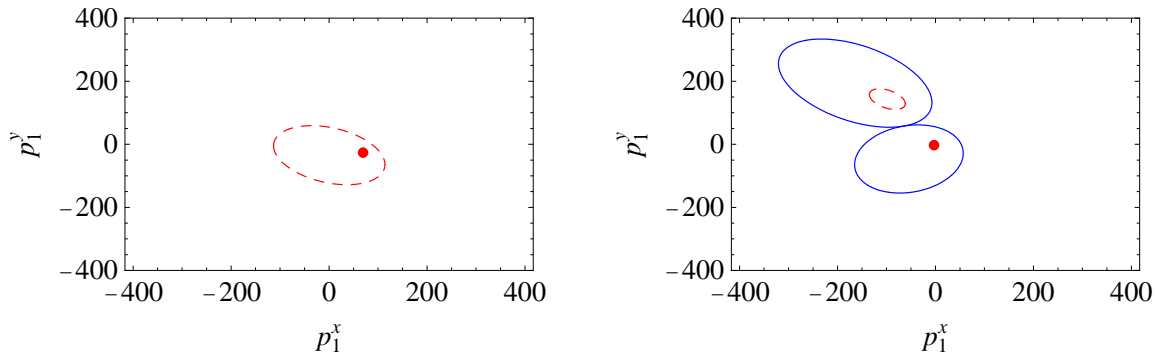


Figure 2: The unbalanced solution (left) and the balanced solution (right). The red (dashed) ellipse and the red point are the two ellipses when $\mu_Y = \mu_N + m_a$. For the unbalanced solution, the point is inside the red ellipse, and $m_{T2} = \mu_N + m_a$. For the balanced solution, the point is outside the red ellipse, and m_{T2} is given when the two ellipses (solid blue) are tangent to each other.

The other decay chain is completely analogous, and we obtain another elliptical region for (p_2^x, p_2^y) . However, the two decay chains are related by the measured \not{p}_T . Therefore, we can eliminate p_2^x and p_2^y to put the second elliptical region also on the (p_1^x, p_1^y) plane. In order to satisfy all the constraints, the two elliptical regions must overlap. Since that the two ellipses both expand as we increase μ_Y , m_{T2} will be given by the minimal μ_Y when the two elliptical regions start to overlap. To proceed we need to distinguish two cases, which are illustrated in Fig. 2 and discussed below.

We assume $m_a \geq m_b$ for the invariant masses of a and b without loss of generality. We see that we must have $\mu_Y \geq \mu_N + m_a$, otherwise the first ellipse vanishes. When $\mu_Y = \mu_N + m_a$, the first ellipse becomes a point, while the second ellipse has a finite size (or is also a point if $m_a = m_b$). If the point (first ellipse of zero size) is within the second elliptical region, then m_{T2} is simply given by $m_{T2} = m_a + \mu_N$. This is called the “unbalanced configuration” in Ref. [13].

The other possibility is that the point representing the zero-sized first ellipse when $\mu_Y = \mu_N + m_a$ is outside the second ellipse. In this case, we have to increase μ_Y until the two elliptical regions overlap to obtain solutions. m_{T2} is then given by the value of μ_Y when the two ellipses are tangent to each other. This is dubbed the “balanced configuration” [13].

Now it is clear how to calculate m_{T2} . For a given μ_N , we first check if the two ellipses give us an unbalanced configuration when $\mu_Y = \mu_N + m_a$. If so, we have $m_{T2} = \mu_N + m_a$. Otherwise, we need to look for the μ_Y when they are tangent.

The two ellipses are described by two quadratic equations, which can be reduced to a univariate quartic equation. When the ellipses are tangent, the quartic equation has degenerate roots and therefore its discriminant vanishes. The discriminant is in general a 12th order polynomial function of μ_N^2 and μ_Y^2 . This provides an analytical relation between μ_N and $m_{T2}(\mu_N)$ which has not been obtained in the literature before for the case of non-vanishing UTM. Although it would not be the most efficient way to do the calculation, in principle one can numerically solve the polynomial equation and obtain m_{T2} . Of course, there can be more than one real solutions for the equation. One should keep the smallest positive μ_Y as m_{T2} since this is the first time the two ellipses are tangent.

It is convenient to use the discriminant when the UTM vanishes. In this case, the equations are simplified so that the 12th order equation is reduced to a 4th order one, for which analytical solutions are available. This confirms the existence of analytical solutions in the zero UTM case discussed in Ref. [13]. When UTM is nonzero, solving a 12th order equation is numerically slow and unstable. We have developed a faster and more robust algorithm for calculating m_{T2} , which is described in detail in Appendix A. The basic idea is that: we know that the two ellipses do not intersect when $\mu_Y^{\min} = \mu_N + m_a$ and we can also find a μ_Y^{\max} when they do intersect by an educated guess. Then m_{T2} must be within the interval $(\mu_Y^{\min}, \mu_Y^{\max})$. Whether the two ellipses intersect can be tested easily by the Sturm sequence [14]. We repeatedly bisect the interval while keeping the m_{T2} within it, until we reach the desired precision.

In the above discussion, we have assumed that $m_{a,b} > 0$. When either m_a or m_b (or both) vanishes, the corresponding ellipse becomes a parabola, but the treatment remains the same.

3. Mass determination using m_{T2}

The simplest application of m_{T2} is to determine m_Y from the m_{T2} endpoint when m_N is known. However, it is often the case that m_N is also unknown, and we want to determine both masses simultaneously. The merit of m_{T2} is that it corresponds to the *minimal* constraints. Therefore it is always well-defined and calculable, which may prove useful at the early stage of the LHC [15]. If more information is available, we can develop more complicated methods based on m_{T2} .

If each decay chain in the events involves only a single two-body decay, *i.e.*, Y decays to N plus a single visible particle with fixed mass, it is impossible to determine both masses from pure kinematics. If we consider two identical decay chains, the next simplest case is then that each decay chain contains two visible particles, which is illustrated in Fig. 3.

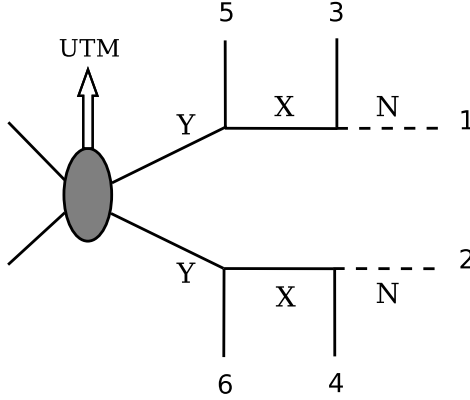


Figure 3: The event topology with 2 visible particles per decay chain. The particle X can be either on shell or off shell.

When the particles in the two decay chains are identical, we can divide the situations into four cases, depending on whether there is significant UTM, and whether the intermediate particle X is on shell or off shell. The latter determines whether the particle Y decays to N through a three-body decay or two consecutive two-body decays. For the two two-body decay cases, we would like to determine m_X as well. The cases with zero or negligible UTM are discussed in Ref. [10]. The authors pointed out that m_{T2}^{\max} , the m_{T2} endpoint value as a function of μ_N , has a kink at $\mu_N = m_N$. In practice, it is difficult to identify the kink due to experimental smearing, but the formula for the m_{T2}^{\max} curve is known, which make it possible to fit the position of the kink.

When the events have significant UTM, the situation is different. UTM can come from initial state radiation or heavier particle decays. For the latter, an example in MSSM is the decay chain

$$\tilde{q} \rightarrow q\tilde{\chi}_2^0 \rightarrow q\ell\tilde{\ell} \rightarrow q\ell\ell\tilde{\chi}_1^0, \quad (3.1)$$

where particles $\tilde{\chi}_2^0$, $\tilde{\ell}$ and $\tilde{\chi}_1^0$ are identified with Y , X and N respectively. The quark from squark decay can be very energetic, providing large UTM to the system. In this case, m_{T2}^{\max} curve is different from the vanishing UTM case and an analytical formula is in general unavailable. We focus on this case in the following, taking the process in (3.1) as an example.

We consider two mSUGRA points, one with $m_{\tilde{\ell}} > m_{\tilde{\chi}_2^0}$ and the other one with $m_{\tilde{\ell}} < m_{\tilde{\chi}_2^0}$, corresponding to the three-body decay case and the two-body decay case respectively. The former is chosen to be the same as the model P1 in Ref. [12] for comparison. The latter is the Snowmass SUSY point SPS1a [16].

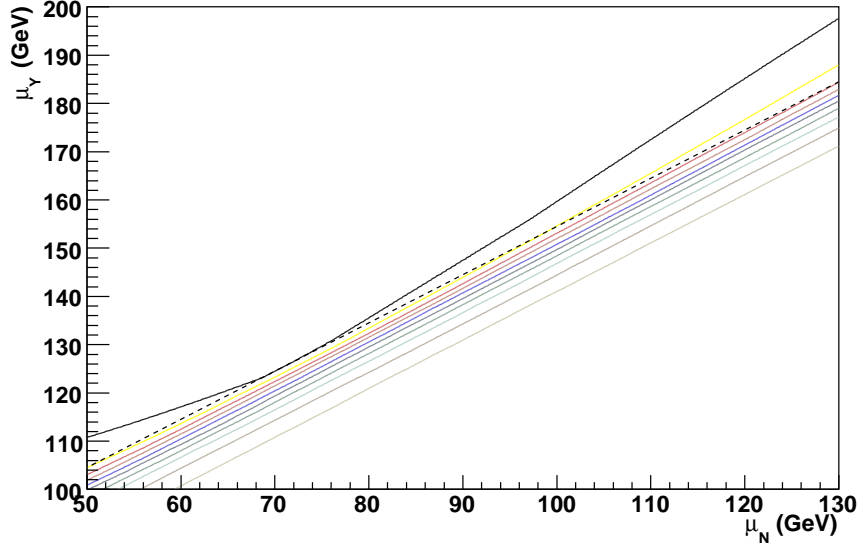


Figure 4: Number of consistent events as a function of (μ_N, μ_Y) for 1000 events, in the three-body decay case. The solid lines are the contours in 100 event intervals, beginning from 1000 for the top contour. The dashed line is the function $\mu_Y - \mu_N = M_-$.

1. $m_0 = 350$ GeV, $m_{1/2} = 180$ GeV, $\tan \beta = 20$, $\text{sign}(\mu) = +$, $A_0 = 0$;
 $m_{\tilde{\chi}_2^0} = 123.7$ GeV, $m_{\tilde{\ell}_R} = 358.6$ GeV, $m_{\tilde{\chi}_1^0} = 70.4$ GeV.
2. $m_0 = 100$ GeV, $m_{1/2} = 250$ GeV, $\tan \beta = 10$, $\text{sign}(\mu) = +$, $A_0 = -100$;
 $m_{\tilde{\chi}_2^0} = 181.0$ GeV, $m_{\tilde{\ell}_R} = 143.7$ GeV, $m_{\tilde{\chi}_1^0} = 100.4$ GeV.

The spectra are calculated with SPheno [17]. We have generated 1000 events for each case with MadGraph/MadEvent at the parton level. In this paper, we will only consider the ideal case, *i.e.*, no background, the particles are exactly on-shell, and there is no experimental smearing or wrong combinatorics for the visible particles. Nevertheless, we have avoided using features that is easily lost after the above effects are included, such as a kink structure, and expect our methods to be valid for realistic cases. A realistic study is left for a future publication.

We first discuss the three-body decay case. Again, it is illuminating to think about m_{T2} as kinematic constraints. We have seen that for one event, the consistent mass region on the (μ_N, μ_Y) plane is above the m_{T2} curve. Using this fact, for multiple events we can easily count the number of events consistent with a given mass point. Fig. 4 is the contour plot for the number of consistent events. In particular, above the uppermost contour, which we identify as the m_{T2}^{max} curve, the masses are consistent

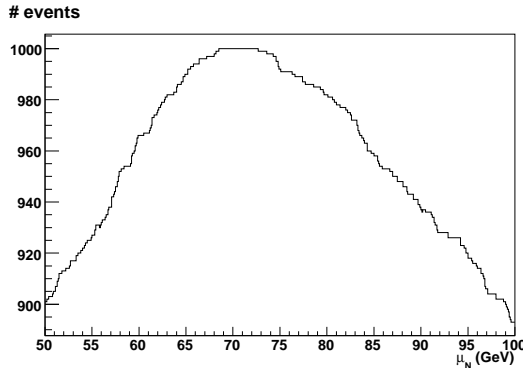


Figure 5: Number of consistent events along the line $\mu_Y - \mu_N = M_-$, in the three-body decay case.

with all 1000 events. A kink structure in the m_{T2}^{\max} curve is visible. However it will be smeared by experimental resolutions and we avoid using it.

Similar to Ref. [12], we can assume that the mass difference $M_- = m_Y - m_N$ is already measured with good precision from the endpoint of the dilepton invariant mass distribution. Indeed, due to branching ratios, it is often the case that there are many more dilepton events than four-lepton events and therefore the mass difference can be measured much better. Drawing a line corresponding to $\mu_Y - \mu_N = M_-$ on the (μ_N, μ_Y) plane, we see that it intersects some of the contours and touches the m_{T2}^{\max} curve only at $\mu_N = m_N$. We can draw the number of consistent events as a function of μ_N , along the line $\mu_Y - \mu_N = M_-$, as shown in Fig. 5. As expected, the number is maximized at $\mu_N = m_N$. This is in some way equivalent to the approach in Ref. [12], where event-by-event lower and upper bounds for m_Y are obtained by intersect the m_{T2} curve with the line $\mu_Y - \mu_N = M_-$. The distribution in Fig. 5 is an integral of the upper and lower bound distributions of Ref. [12]. Presenting in this way allows easy generalizations to other cases. To minimize the statistical error, instead of simply reading the maximum in Fig. 5, we can also fit the distribution to template distributions around the true m_N , analogous to Ref. [12].

We now turn to the two-body decay case. In this case, the particle X is on-shell, which gives us constraints in addition to Eqs. (2.7) (where $p_a = p_3 + p_5$ and $p_b = p_4 + p_6$):

$$(p_1 + p_3)^2 = (p_2 + p_4)^2 = \mu_X^2, \quad (3.2)$$

where μ_X is a trial mass for X . Unlike the minimal constraints, the system given by combining Eqs. (2.7) and (3.2) can be solved event by event to yield discrete solutions

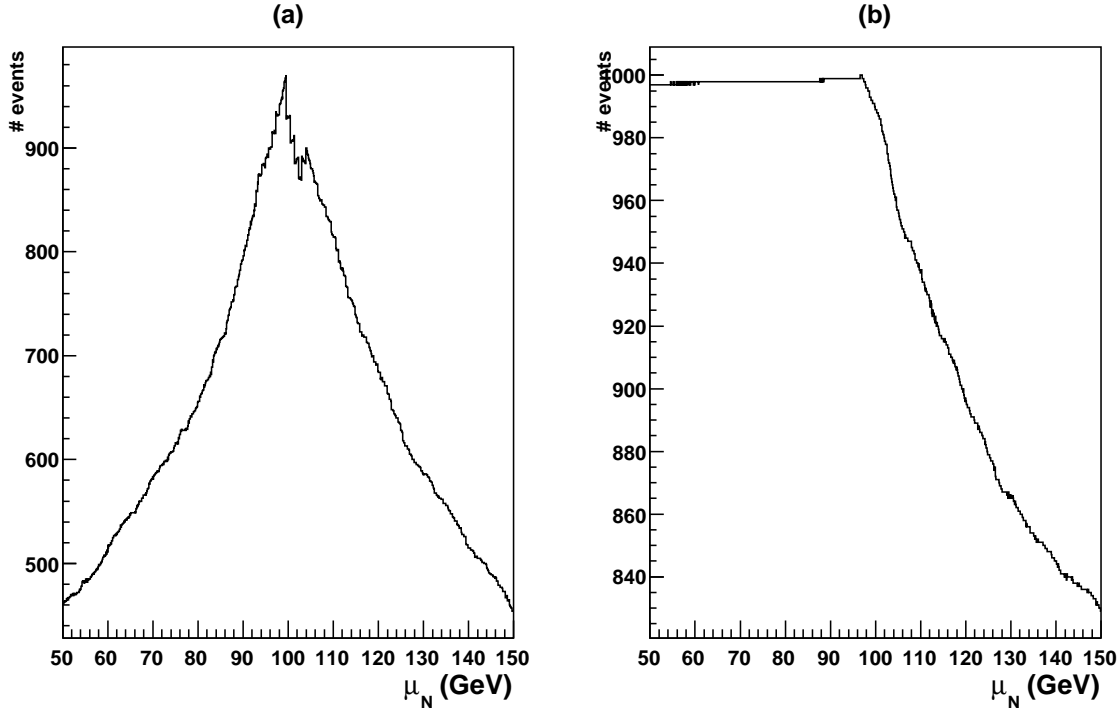


Figure 6: Number of consistent events distribution for $\mu_Y = m_{T2}^{\max}(\mu_N)$, in the two-body decay case. Left: m_X is determined from the edge of the dilepton invariant mass distribution; right: m_X is the value that maximize the number of consistent events.

for p_1 and p_2 (up to a four-fold ambiguity)¹. Depending on whether the solutions are physical, we can determine if an event is consistent with a given set of masses (μ_N, μ_X, μ_Y) . This fact is used in Ref. [6] to determine all three masses by examining the distribution of the number of consistent events. There, the masses are obtained through a series of one-dimensional recursive fits. In the following, we present a simplified method utilizing the m_{T2}^{\max} curve. The idea is that we can follow the m_{T2}^{\max} curve, which gives us a relation between m_Y and m_N , and count the number of consistent events. Depending on whether we want to use measurement from the dilepton invariant mass distribution like in the off-shell case, the method is slightly different.

It is well known that for the decay chain in (3.1) with $\tilde{\ell}$ on shell, there is a sharp edge in the dilepton invariant mass distribution at

$$m_{\ell\ell}^2|_{edge} = \frac{(m_Y^2 - m_X^2)(m_X^2 - m_N^2)}{m_X^2}. \quad (3.3)$$

¹This fact was first used to study $t\bar{t}$ events in the dilepton channel, see, for example, Ref. [18].

Assuming the edge position is measured with good precision, we obtain a relation among the three trial masses. Together with the relation from m_{T2}^{\max} curve, μ_X and μ_Y are fixed for a given μ_N , up to a two-fold ambiguity from inversion of Eq. (3.3). Then the number of events consistent with Eqs. (2.7) and (3.2), as a function of μ_N is given in Fig. 6 (a). There is an evident peak at $\mu_N = m_N$.

The masses can be determined without using the measurement of the $m_{\ell\ell}$ edge. For each μ_N , we first fix μ_Y by the m_{T2}^{\max} function. Then we *vary* μ_X to maximize the number of consistent events. This maximum number is shown in Fig. 6 (b), as a function of μ_N^2 . Unlike the previous case, there is not a peak structure, but the number of events drops sharply when $\mu_N > m_N$, which can be used to estimate the masses.

4. Discussion and conclusions

We have demonstrated the relation between the m_{T2} variable and the kinematic constraints for events with two identical decay chains, each of which ends up with one missing particle. The m_{T2}^{\max} curve is equivalent to the boundary of the consistent region in the mass space from the minimal kinematic constraints, where only the mass shell conditions of the decaying mother particles and the final missing particles, and the measured missing transverse momentum constraint are imposed. In fact, it should not be surprising that many different mass determination methods are closely related since they are based on the same kinematics. Understanding their relations may allow us to develop more effective and powerful ways for mass determination either by finding new strategies or by combining various approaches. Here we will try to give a general discussion of the mass determination program based solely on kinematics.

For a given topology of new physics events, we can think of it as a map between the “mass” space \mathcal{M} and the “observable” space \mathcal{O} . The mass space is the space of the mass parameters of the new particles which appear on shell in those events. The dimension is equal to the number of the unknown masses that are to be determined. The observable space is the multi-dimensional space of *all* independent kinematic observables which are relevant for the mass determination in those events. Basically, they are made of the momenta of the visible particles (jets and leptons) from the decay chains, and the missing transverse momentum. Therefore, each experimental event can be represented by a point in the observable space. In principle we can choose any basis for the observable space. It is convenient, however, to choose combinations that are invariant under

²When $m_{T2}^{\max}(\mu_N) < m_Y$, which is always the case for finite number of events, the number of solvable events at $\mu_N = m_N$ drops much below the maximum number. Therefore, in Fig. 6 (b) we have added to μ_Y a small constant, $\mu_Y = m_{T2}^{\max} + 2$ GeV.

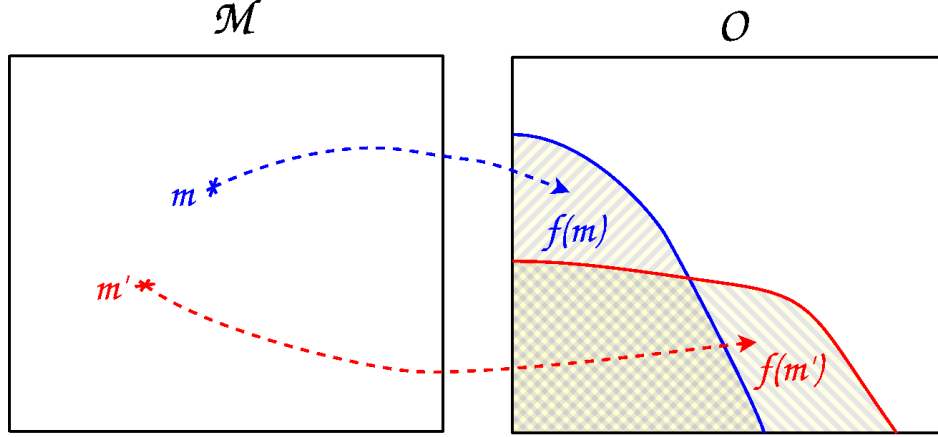


Figure 7: The map between a point in the mass space and the corresponding consistent region in the observable space.

certain transformations which do not alter the connection between the mass parameters and the kinematic observables. For example, if an event of certain observable momenta can be produced by some mass parameters, a boost along the beam axis can also be produced by the same mass parameters because the momenta along the beam axis and the energies of the initial partons in collision are unknown. They do not have to be fully Lorentz-invariant as the measured missing transverse momentum breaks the symmetry. For two decay chains in an event which is the focus of most discussion, the allowed transformations are independent boosts of the two decay chains along the beam axis and the rotation around the beam axis, so it would be advantageous to choose the observable combinations that are invariant under these transformations. (If there is no UTM, one can also perform back-to-back equal transverse boosts on the two chains as the two mother particles have equal and opposite transverse momenta in this case.)

For each point \mathbf{m} in the mass space, there is a corresponding region $f(\mathbf{m}) \subset \mathcal{O}$ in the observable space which is consistent with this mass point, *i.e.*, $f(\mathbf{m})$ is made of all possible points in the observable space that can be produced kinematically by the given mass parameters (see Fig. 7). Assuming that there is a large enough set of experimental events from this topology with the given mass parameters at \mathbf{m} and ignoring the issues such as experimental smearing and backgrounds for the moment, the region $f(\mathbf{m})$ will be populated by these experimental events. The relative weights and densities of the experimental events within the region depend on other details of the underlying theory such as the matrix elements. On the other hand, the allowed region $f(\mathbf{m})$ solely depends on the masses of the new particles. If $f(\mathbf{m})$ is unique for each point \mathbf{m} , then in principle

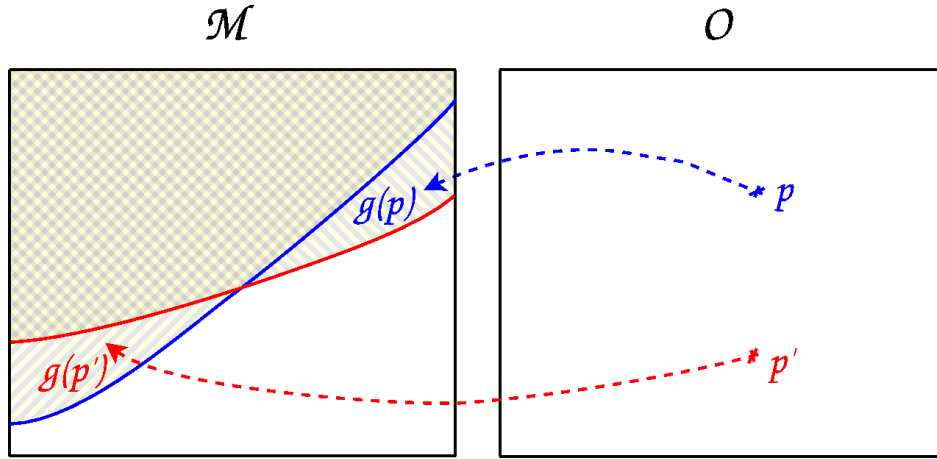


Figure 8: The map between a point in the observable space and the corresponding consistent region in the mass space.

all the masses can be uniquely determined given enough of experimental events. It is possible that there are degeneracies such that different mass points map into the same observable region, $f(\mathbf{m}) = f(\mathbf{m}')$ for $\mathbf{m} \neq \mathbf{m}'$, *e.g.*, the case of one step two-body decay on each chain. In that case the masses cannot be uniquely determined from kinematics alone and additional (model-dependent) information is required. In general we expect $f(\mathbf{m})$ to be unique if the dimension of the observable space is large enough. From the above discussion, we see that the most important events for mass determination are those which lie near the boundary of $f(\mathbf{m})$ as they determine the shape and the size of $f(\mathbf{m})$. The edge/endpoint method can be viewed as a simple application of this idea by projecting $f(\mathbf{m})$ down to a few one-dimensional subspaces and extract the endpoints of $f(\mathbf{m})$ in these one-dimensional subspaces. It is also evident that it does not fully utilize all the relevant information contained in the experimental events as it only uses a few points on the boundary. In particular, in the case of two visible particles in each decay chain it does not give enough information to determine all masses, yet we know that the masses can be determined by other methods. A generalization to look at the boundary of the two-dimensional subspaces of $f(\mathbf{m})$ is currently being studied [19]. It can potentially give a more powerful method than the one-dimensional endpoint method. Ideally, one would like to map out the whole boundary of $f(\mathbf{m})$ in the high-dimensional observable space to get all the information contained in the experimental events. However, dealing with the high-dimensional space could be technically quite difficult.

The method of kinematic constraints can be considered as the inverse map of the

mass space and the observable space discussed above. Each experimental signal event which is represented by a point \mathbf{p} in the observable space \mathcal{O} can define a region $g(\mathbf{p})$ in the mass space \mathcal{M} which is consistent with that event (see Fig. 8). Obviously, $\mathbf{m} \in g(\mathbf{p})$ if and only if $\mathbf{p} \in f(\mathbf{m})$. The correct mass point must lie within the region $g(\mathbf{p})$ assuming that the event is a valid signal event and no experimental smearing. By combining many experimental events we can find the intersection of all $g(\mathbf{p}_i)$ for all experimental points \mathbf{p}_i ,

$$G(E) = \bigcap_{\mathbf{p}_i \in E} g(\mathbf{p}_i), \quad (4.1)$$

where E is the region in the observable space occupied by the experimental events. If there are sufficiently many events, we expect $E = f(\mathbf{m}_{\text{true}})$ for the correct mass point \mathbf{m}_{true} . For certain event topologies, *e.g.*, three on-shell two-body decays for each decay chain [7], the intersection region shrinks to a point after combining a finite number of events. Obviously it would correspond to the correct mass point, $G(E) = \{\mathbf{m}_{\text{true}}\}$, and the mass determination is conceptually straightforward in this case. Of course in practice, such determination will be complicated by experimental smearing, backgrounds, and combinatorics. Non-trivial techniques still need to be developed to resolve these issues in order to demonstrate the viability and accuracies of mass determination in this way. On the other hand, for many other topologies the region in the mass space consistent with all experimental events $G(E)$ remains finite. Naïvely one might think that this is a degeneracy and the masses cannot be uniquely determined. However, a point in the mass space \mathbf{m} that is consistent with all events only implies that $f(\mathbf{m}) \supset E$. For a generic but not the true mass point in $G(E)$, $f(\mathbf{m})$ will be larger than E . Assuming that the map between the two spaces is continuous, we then expect that its immediate neighborhood points \mathbf{m}' in many directions will still be consistent with all events, $f(\mathbf{m}') \supset E$. From this argument we see that any point lying in the middle of $G(E)$ will not be the true mass point. For the true mass point, we should have $f(\mathbf{m}_{\text{true}})$ coincide exactly with E . Such a point would have the least neighborhood points which are still consistent with all events, or said in another way, it has the least degrees of freedom to move while staying within $G(E)$. This tells us that the true mass point should lie on the boundary of the consistent mass region $G(E)$. In particular, if there is a sharp edge or a “kink” on the boundary of $G(E)$, it would be a good candidate for the true mass point. This fact has been used to develop a new method for mass determination in Ref. [6]. Now we see that the method of the m_{T2} kink [10, 11] is another example, as the m_{T2}^{max} curve is just the boundary of the consistent region in the two-dimensional mass (sub)space based on the minimal kinematic constraints. These methods effectively attempt to match the whole region of $f(\mathbf{m})$ with the region of experimental events E as we hope to achieve in our discussion

in the previous paragraph.

In the realistic situation, such a sharp edge or “kink” of the consistent mass region can easily be washed out after the experimental smearing and backgrounds are taken into account. Therefore it may not be practical to directly search for the kink position. However, understanding the structure of the consistent mass region from the kinematic constraints allows us to develop strategies to recover the kink location by combining various techniques that people have developed. For example, it is well known that for collider signal events with missing energies, the difficulty is to determine the overall mass scale. The relative masses or mass differences usually can be well constrained from the kinematic variables such as the endpoints of invariant masses of visible particles. We can use those kinematic variables to reduce the mass space down to a one (or low) dimensional space which contains the true mass point. Then if we count the number of consistent events as a function of the points along this one dimensional space, it would, in the idealized case, exhibit a sharp turning in number of consistent events at the true mass point due to the “kink” nature of the consistent mass region near that point. Even though the sharpness of the turning point will be reduced by the experimental smearing and the presence of backgrounds, this “turning” feature is expected to survive as long as we have a reasonable data set of the signal events, and we can fit for the turning point to determine the overall mass scale. This was illustrated in Section 3.

In conclusion, we have clarified the relation between the m_{T2} variable and the kinematic constraints for events with two decay chains ending with invisible particles. m_{T2} is a clever variable which simply corresponds to the boundary of the allowed mass region from the minimal kinematic constraints where only the constraints of mass shell conditions of the mother particles and the missing particles of the two decay chains, and the measured missing transverse momentum are used. As a by-product, we also found a faster algorithm to calculate m_{T2} from the point of view of kinematic constraints. These connections can also tell us how to develop new ways by combining different existing methods to achieve the more powerful and accurate mass determination for events with missing energies. It will be extremely important for reconstructing the underlying theory and verifying whether we have discovered the dark matter particle if such new physics events with missing energies are indeed found at the LHC.

Acknowledgments

This work is supported in part by the U.S. Department of Energy grant No. DE-FG02-91ER40674.

A. The bisection method for calculating m_{T2}

We describe in this appendix the bisection algorithm for calculating m_{T2} for the balanced configuration.

First, we need a method to quickly determine if two ellipses intersect, *without* solving the quartic equation described in Section 2.3. This is done by calculating the Sturm sequence for the quartic polynomial, which gives us the number of real solutions for the quartic equation [14]. When the number of real solutions are zero, either the two ellipses are outside each other, or one completely contains the other one.

For the balanced configuration, the two ellipses are outside each other for $\mu_Y^{\min} = \mu_N + \max\{m_a, m_b\}$. When we increase μ_Y , both ellipses expand. It is easy to see that they always intersect for μ_Y in some range. Thus, we need to guess a point when they intersect. We do this by first finding a μ_Y such that the two ellipses enclose a same point, for example, the origin. In this case, either they intersect or one contains the other one. If it is the former, we have found an intersecting point which is taken as μ_Y^{\max} . If it is the latter, which rarely happens, we need to do a scan from μ_Y^{\min} to find the intersecting point.

After obtaining μ_Y^{\min} and μ_Y^{\max} , we bisect the interval $(\mu_Y^{\min}, \mu_Y^{\max})$ and check if the two ellipses intersect at the middle point of the interval $\mu_Y^{\text{mid}} = (\mu_Y^{\min} + \mu_Y^{\max})/2$. If yes, we set the new $\mu_Y^{\max} = \mu_Y^{\text{mid}}$; otherwise, $\mu_Y^{\min} = \mu_Y^{\text{mid}}$. We repeat this procedure until the size of the interval is smaller than the precision we want.

The algorithm has been implemented in c++ and available at Ref. [20] or from the authors. The code has been tested for 250k events. These include 5 datasets with 50k events each corresponding to the $t\bar{t}$ production in the dilepton channel, and the two SUSY mass points discussed in Section 3. For the SUSY points, events with UTM (from squark pair production and decay) and without UTM (from direct $\tilde{\chi}_2^0$ pair production) are tested separately. The tests are performed for a variety of trial masses μ_N . The results have been compared with Ref. [21], showing good agreement in the numerical values of m_{T2} : the possibility is $O(10^{-5} \sim 10^{-4})$ for the two programs to yield values that differ by 1 GeV or more, and $O(10^{-4} \sim 10^{-3})$ for 0.1 GeV or more. For the events that give small differences, our code is showing more accurate results, which can be verified in Mathematica by examining when the two ellipses are tangent to each other. Our code is also much faster (5–9 times as fast as Ref. [21]), making it advantageous when m_{T2} needs to be repeatedly calculated, for example, in evaluation of the $m_{T\text{Gen}}$ variable [13].

References

- [1] T. Appelquist, H. C. Cheng and B. A. Dobrescu, Phys. Rev. D **64**, 035002 (2001) [arXiv:hep-ph/0012100]; H. C. Cheng, K. T. Matchev and M. Schmaltz, Phys. Rev. D **66**, 056006 (2002) [arXiv:hep-ph/0205314].
- [2] H. C. Cheng and I. Low, JHEP **0309**, 051 (2003) [arXiv:hep-ph/0308199]; H. C. Cheng and I. Low, JHEP **0408**, 061 (2004) [arXiv:hep-ph/0405243].
- [3] I. Hinchliffe, F. E. Paige, M. D. Shapiro, J. Soderqvist and W. Yao, Phys. Rev. D **55**, 5520 (1997) [arXiv:hep-ph/9610544].
- [4] H. Bachacou, I. Hinchliffe and F. E. Paige, Phys. Rev. D **62**, 015009 (2000) [arXiv:hep-ph/9907518]; B. C. Allanach, C. G. Lester, M. A. Parker and B. R. Webber, JHEP **0009**, 004 (2000) [arXiv:hep-ph/0007009]; B. K. Gjelsten, D. J. Miller and P. Osland, JHEP **0412**, 003 (2004) [arXiv:hep-ph/0410303]; C. G. Lester, Phys. Lett. B **655**, 39 (2007) [arXiv:hep-ph/0603171].
- [5] K. Kawagoe, M. M. Nojiri and G. Polesello, Phys. Rev. D **71**, 035008 (2005) [arXiv:hep-ph/0410160].
- [6] H. C. Cheng, J. F. Gunion, Z. Han, G. Marandella and B. McElrath, JHEP **0712**, 076 (2007) [arXiv:0707.0030 [hep-ph]].
- [7] H. C. Cheng, D. Engelhardt, J. F. Gunion, Z. Han and B. McElrath, Phys. Rev. Lett. **100**, 252001 (2008) [arXiv:0802.4290 [hep-ph]].
- [8] M. M. Nojiri, G. Polesello and D. R. Tovey, JHEP **0805**, 014 (2008) [arXiv:0712.2718 [hep-ph]].
- [9] C. G. Lester and D. J. Summers, Phys. Lett. B **463**, 99 (1999) [arXiv:hep-ph/9906349]; A. Barr, C. Lester and P. Stephens, J. Phys. G **29**, 2343 (2003) [arXiv:hep-ph/0304226].
- [10] W. S. Cho, K. Choi, Y. G. Kim and C. B. Park, Phys. Rev. Lett. **100**, 171801 (2008) [arXiv:0709.0288 [hep-ph]]; W. S. Cho, K. Choi, Y. G. Kim and C. B. Park, JHEP **0802**, 035 (2008) [arXiv:0711.4526 [hep-ph]].
- [11] A. J. Barr, B. Gripaios and C. G. Lester, JHEP **0802**, 014 (2008) [arXiv:0711.4008 [hep-ph]].
- [12] G. G. Ross and M. Serna, Phys. Lett. B **665**, 212 (2008) [arXiv:0712.0943 [hep-ph]]; A. J. Barr, G. G. Ross and M. Serna, arXiv:0806.3224 [hep-ph].
- [13] C. Lester and A. Barr, JHEP **0712**, 102 (2007) [arXiv:0708.1028 [hep-ph]].
- [14] D. Eberly, <http://www.geometrictools.com/Documentation/IntersectionOfEllipses.pdf>.

- [15] M. M. Nojiri, Y. Shimizu, S. Okada and K. Kawagoe, JHEP **0806**, 035 (2008) [arXiv:0802.2412 [hep-ph]]; M. M. Nojiri, K. Sakurai, Y. Shimizu and M. Takeuchi, arXiv:0808.1094 [hep-ph].
- [16] B. C. Allanach *et al.*, in *Proc. of the APS/DPF/DPB Summer Study on the Future of Particle Physics (Snowmass 2001)* ed. N. Graf, *In the Proceedings of APS / DPF / DPB Summer Study on the Future of Particle Physics (Snowmass 2001)*, Snowmass, Colorado, 30 Jun - 21 Jul 2001, pp P125 [arXiv:hep-ph/0202233].
- [17] W. Porod, Comput. Phys. Commun. **153**, 275 (2003) [arXiv:hep-ph/0301101].
- [18] V. Simak, P. Homola, J. Valenta and R. Leitner, ATL-PHYS-2001-018; L. Sonnenschein, Phys. Rev. D **73**, 054015 (2006) [arXiv:hep-ph/0603011]; Y. Bai and Z. Han, arXiv:0809.4487 [hep-ph].
- [19] Talks by M. E. Burns and M. Park at Pheno 2008 Symposium, University of Wisconsin; M. E. Burns, K. T. Matchev, and M. Park, to appear.
- [20] <http://daneel.physics.ucdavis.edu/~zhenyuhan/mt2.html>
- [21] A. Barr and C. Lester, <http://www.hep.phy.cam.ac.uk/~lester/mt2/index.html>. The code used for comparison is *Basic-Mt2-332-Calculator*.